We are IntechOpen,
the world's leading publisher of
Open Access books
Built by scientists, for scientists

4,800
Open access books available

122,000
International authors and editors

135M
Downloads

Our authors are among the

154
Countries delivered to

TOP 1%
most cited scientists

12.2%
Contributors from top 500 universities

BOOK CITATION INDEX
CLARIVATE ANALYTICS
INDEXED

WEB OF SCIENCE™

Selection of our books indexed in the Book Citation Index
in Web of Science™ Core Collection (BKCI)

Interested in publishing with us?
Contact book.department@intechopen.com

Numbers displayed above are based on latest data collected.
For more information visit www.intechopen.com

Enhanced Molecular Spectroscopy via Localized Surface Plasmon Resonance

Lu Sun, Ping Chen and Lie Lin

Additional information is available at the end of the chapter

Abstract

Numerous novel spectroscopy techniques have been developed to perform detection and characterization at molecular level. Nevertheless, the resolution of spectroscopy remains to be the bottleneck, and local electric field is involved to solve this issue. Localized surface plasmon resonance (LSPR) occurred at the surface of noble metal nanoparticles is a major source of enhanced local electric field which provide notable enhancement factor of spectroscopy applying fluorescence and the Raman scattering. In this chapter, we will firstly present the physics of localized surface plasmon resonance to gain a basic understanding. Several current techniques to prepare a wide variety of nanoparticles and localized surface plasmon resonance detector are subsequently introduced. We further illustrate two examples taking advantage of experiments and modeling to elaborate the effect of localized surface plasmon resonance on spectroscopy under different circumstances. The combination of experimental and theoretical approaches elucidates the influence of each factor and promotes the design of localized surface plasmon resonance detector used in spectroscopy.

Keywords: spectroscopy, localized surface plasmon resonance, nanoparticle, detection, enhancement factor, finite-difference time-domain

1. Introduction

The advance of science and technology has drawn people's attention to the molecular level, and characterization of molecular configuration is among the most significant challenges. Spectroscopy takes advantage of the interaction between electromagnetic radiation and matter and records the response of interest. The resulting spectrum containing the fingerprint of the analyte sheds light on specific structural details of a single molecule.

State-of-the-art spectroscopy techniques employing fluorescence [1], the Raman scattering [2], X-ray [3], NMR [4], etc. have been successfully utilized to illustrate the conformations of biomolecules such as protein, DNA, and RNA. Moreover, utilizing lasers with impulse interval at femtosecond as excitation power has accomplished ultrafast detections. For example, the instantaneous structures of mRNA-tRNA translocation intermediates have been characterized through single-molecule fluorescence resonance energy transfer method, the achievement of which is a huge step toward the comprehensive mechanism of in vivo protein synthesis [5].

Despite the pronounced temporal resolution achieved during the past two decades, the spatial resolution is another key issue to fulfill detection and characterization at the single-molecule level. For instance, the cross section of non-resonant Raman scattering is typically ranging from 10^{-30} to 10^{-25} cm^2 per molecule, a value so weak that a notable amount of analyte molecules is demanded to convert the incident photon to the Raman photon [6]. Although the laser power still has the potent to be augmented, the loss during transmission is too dramatic to exert a distinct influence by simply replacing an intensified laser. Local electromagnetic field is therefore more applicable in enhancing the resolution of spectroscopy.

The progress of nanoparticles' localized surface plasmon resonance (LSPR) is becoming a major solution to enhance the intensity of engendered signals through the highly localized electromagnetic field. It has been discovered that the electrons within the conduction band can be excited collectively at noble metal surface and the consequential oscillation of the excited electrons would be localized instead of propagating on a rough surface [7].

Extensive studies have been conducted to manipulate LSPR at the surface of different kinds of nanoparticles, and LSPR has displayed distinct properties by regulated size, shape, structure, material, and other factors [8]. For example, it has been shown that the wavelength of plasmon varies with the particle radius [9], two distinguished plasmonic radiations have been found in nano-rod [10], and aggregates of nanoparticles show more localized optical field with hot spots and cold zones compared with isolated nanoparticles [11].

Together with the significant improvement in the fabrication of a variety of nanostructures during last decade, gold- and silver-nanostructures generating LSPR are nowadays applicable and have been integrated into sensors and detectors [12, 13] Surface-enhanced Raman spectroscopy has recently made detection of biological and chemical analytes with concentration as low as nanogram and femtogram feasible [14]. For different nanostructures, enhancement effect of LSPR cannot be predicted instinctively but through theoretical methods such as finite-difference time-domain (FDTD), discrete dipole approximation (DDA), and finite element method (FEM) [15].

In this chapter, we elaborate the efficacy of researches applying experimental techniques and computation modeling to enhance spectroscopy through LSPR. We first interpret the physics that originated LSPR. Since LSPR occurs at the surface of nanoparticles, different ways to fabricate nanostructure in order to generate LSPR and how nanoparticles are used as detector are thereafter introduced. Finally, examples of studies applying LSPR to enhance molecular spectroscopy and interpretations through finite-difference time-domain simulations are illustrated.

2. Physics of localized surface plasmon resonance

The observation of surface plasmon could be dated back to the beginning of the last century when Wood observed the anomalous light diffraction on a metallic diffraction grating, a phenomenon later proved to be correlated with the excitation of electromagnetic waves on the surface of the diffraction grating [16]. The plasmon generated from the collective oscillation of the free electrons can be described by the classical Maxwell's equation. We can treat the plasmon as the mechanical oscillations of the electron gas of a metal resulted from an external electric field. For the bulk system with size larger than the wavelength of the incident light, the oscillations occur at the plasma frequency with the energy:

$$E_{\mathrm{p}} = \hbar \sqrt{\frac{ne^2}{m\varepsilon_0}} \tag{1}$$

where n denotes the electron density, e is the electron charge, m is the electron mass, and ε_0 represents the permittivity of free space.

Under this circumstance, the oscillations of electrons are simply called surface plasmons. Surface plasmons can be excited through incident light. A light can couple with a surface plasmon at a metal-dielectric interface only if the incidence angle meets the criteria, because the wavevector of the incident light should accord with the propagation constant of the plasmon so that the oscillating electric field of the incident light is capable of exciting surface plasmons. The application of surface plasmon is therefore limited.
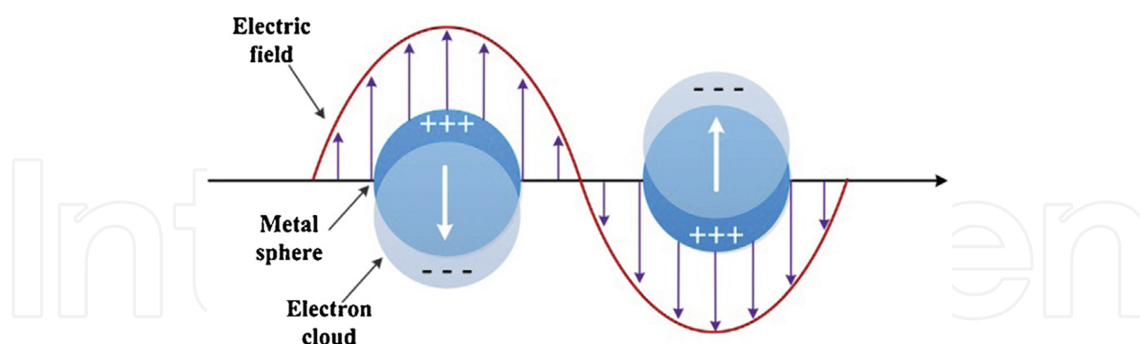

Figure 1. Illustration of the excitation of localized surface plasmon resonance [17].

However, when a surface plasmon is excited at the surface of a metallic nanoparticle with the size comparable to the wavelength of light, the free electrons are confined and take parts in the collective oscillations. This kind of oscillation is thus termed as localized surface plasmon (LSP), with the oscillation shown in **Figure 1**. Since the oscillation is collective, the LSP has taken advantage of significant enhancement at the surface. It is worth noticing that the magnitude of the field attenuates drastically with the distance to the surface of the nanoparticle.

Moreover, the size of nanoparticle makes the frequency of LSP, which also depends on the refractive index of the medium, at visible wavelengths for noble metal nanoparticles.

Since the size of nanoparticle is comparable to the wavelength of light, the Mie theory for light scattering would be considered. Through the analytical solution to Maxwell's equation in the Mie theory, the scattering, extinction, and absorption cross sections are solved as

$$C_{sca} = \frac{2\pi}{k^2} \sum_{N=1}^{\infty} (2N+1)\left(|a_n|^2 + |b_n|^2\right) \tag{2}$$

$$C_{ext} = \frac{2\pi}{k^2} \sum_{N=1}^{\infty} (2N+1)\mathrm{Re}\{a_n + b_n\} \tag{3}$$

$$C_{abs} = C_{ext} - C_{sca} \tag{4}$$

where k is the incident wavevector, N is an integer representing the dipole, quadrupole, and higher multipoles of the scattering, a_L and b_L are the parameters represented by the Riccati-Bessel functions ψ_L and ξ_L expressed below:

$$a_n = \frac{m\psi_n(mx)\psi_n{}'(x) - \psi_n(x)\psi_n{}'(mx)}{m\psi_n(mx)\xi_n{}'(x) - \xi_n(x)\psi_n{}'(mx)} \tag{5}$$

$$b_n = \frac{\psi_n(mx)\psi_n{}'(x) - m\psi_n(x)\psi_n{}'(mx)}{\psi_n(mx)\xi_n{}'(x) - m\xi_n(x)\psi_n{}'(mx)} \tag{6}$$

$$m = \frac{n_p}{n_m} \tag{7}$$

where n_p is the complex refractive index of the metal utilized and is equivalent to n_r+in_i, n_m is the real refractive index of the medium, and x equals to $k_m r$ (r is the radius of the particle, $k_m=2\pi/\lambda_m$ indicates the wave number in the medium).

To simplify the equation, Riccati-Bessel functions can be approximated by power series if we assume the nanoparticle is much smaller compared to the wavelength (i.e., $x \ll <1$). By truncating terms after the order of x^3, we have

$$a_1 \approx -\frac{i2x^3}{3}\frac{m^2-1}{m^2+2} \tag{8}$$

$$b_1 \approx 0 \tag{9}$$

The real part of a_1 required to calculate the cross section of extinction can be found by replacing $m = \dfrac{n_r + in_i}{n_m}$ into a_1 as

$$a_1 \approx -\frac{i2x^3}{3}\frac{m^2-1}{m^2+2} = -\frac{i2x^3}{3}\frac{n_r^2 - n_i^2 + i2n_r n_i - n_m^2}{n_r^2 - n_i^2 + i2n_r n_i + 2n_m^2} \tag{10}$$

Further substituting the dielectric function of metal with the complex form

$$\varepsilon_p = \varepsilon_1 + i\varepsilon_2 \tag{11}$$

$$\varepsilon_1 = n_r^2 - n_i^2 \tag{12}$$

$$\varepsilon_2 = 2n_r n_i \tag{13}$$

and replacing the dielectric function of medium, $\varepsilon_m = n_m^2$, will result in the following relation as

$$a_1 = -\frac{i2x^3}{3}\frac{\varepsilon_1^2 + \varepsilon_1\varepsilon_m - 3\varepsilon_2\varepsilon_m + \varepsilon_2^2 - 2\varepsilon_m^2}{\left(\varepsilon_1 + \varepsilon_m\right)^2 + \varepsilon_2^2} \tag{14}$$

Substituting the above equation into the extinction cross section and only taking the dipole term, we can get the most quoted expression for LSPR as

$$C_{ext} = \frac{18\pi\varepsilon_m^{\frac{3}{2}}V}{\lambda}\frac{\varepsilon_2(\lambda)}{\left[\varepsilon_1(\lambda) + 2\varepsilon_m\right]^2 + \varepsilon_2(\lambda)^2} \tag{15}$$

In here, V represents the volume of the particle. Similarly, the scattering cross section can be expressed as

$$C_{sca} = \frac{34\pi^4\varepsilon_m^2 V^2}{\lambda^4}\frac{\left(\varepsilon_1 - \varepsilon_m\right)^2 + \varepsilon_2^2}{\left(\varepsilon_1 + 2\varepsilon_m\right)^2 + \varepsilon_2^2} \tag{16}$$

Because we supposed that the nanoparticles are small enough to use the approximation, the equation above would be strictly applied to particles with diameter smaller than 10 nm. Nevertheless, it is noteworthy that the expression will give certain accuracy for larger particles as well [18].

The functional form of the LSPR peak wavelength is dependent on the dielectric function of the medium [19], and the dependence can be derived by the following access.

The frequency-dependent dielectric constant for ε_1 according to the Drude model of the electronic structure of metal would be

$$\varepsilon_1 = 1 - \frac{\omega_p^2}{\omega^2 + \gamma^2} \tag{17}$$

in which ω_p denotes the plasma frequency and γ represents the damping parameter of the bulk metal. It is notable the Drude model is a classical model of electronic transport in conductors and describes the collisions between freely moving electrons and the lattice of heavy, stationary ionic cores. The model is a very good approximation for the conductivity of noble metals. For visible and near-infrared frequencies, where $\gamma \ll \omega_p$, the above relation would be reduced to the following form as

$$\varepsilon_1 = 1 - \frac{\omega_p^2}{\omega^2} \tag{18}$$

Substituting the above expression for ε_1 and setting $\varepsilon_1 = -2\varepsilon_m$ as the resonance condition, we can obtain the maximum peak of the LSPR frequency as

$$\omega_{max} = \frac{\omega_p}{\sqrt{2\varepsilon_m + 1}} \tag{19}$$

Because the relation between frequency and wavelength is denoted as $\lambda = 2\pi c/\omega$, the wavelength of LSPR can be expressed after replacing the dielectric constant with the refraction $\varepsilon_m = n^2$:

$$\lambda_{max} = \lambda_p \sqrt{2n_m^2 + 1} \tag{20}$$

in which λ_{max} is the peak wavelength of LSPR while λ_p represents the corresponding wavelength to the plasma frequency of the bulk metal.

Because the nanoparticles generating LSPR are generally not strictly spherical, Richard Gans further complemented the Mie theory to spheroidal particles of any aspect ratio in the small

particle approximation. The absorption cross section for a prolate spheroid (nanorod structure) is found analogous to that of the spherical nanoparticles, as

$$C_{abs} = \frac{\omega}{3c} \varepsilon_m^{\frac{3}{2}} V \sum_j \frac{\left(1/P_j^2\right)\varepsilon_2}{\left[\varepsilon_1 + \frac{\left(1-P_j\right)\varepsilon_m}{P_j}\right]^2 + \varepsilon_2^2} \tag{21}$$

The sum over j infers to the three dimensions of the nanoparticle. P_j denoting the depolarization factors has three components, P_A, P_B, and P_C, along each axis. For a prolate spheroid with aspect ratio A > B = C, the depolarization factors alter the dielectric constant ε_1 and ε_2 anisotropically. Therefore, the corresponding LSPR peak frequencies are different at different directions. The depolarization factors are expressed as

$$P_A = \frac{1-e^2}{e^2}\left[\frac{1}{2e}\ln\left(\frac{1+e}{1-e}\right)-1\right] \tag{22}$$

$$P_B = P_B = \frac{1-P_A}{2} \tag{23}$$

where e is the ellipticity factor that includes the particle aspect ratio R:

$$e = \sqrt{1-\left(\frac{B}{A}\right)^2} = \sqrt{1-\left(\frac{1}{R}\right)^2} \tag{24}$$

The extinction spectrum resulting from nanorod has two peaks, one corresponding to the transverse plasmon mode and the other corresponding to the longitudinal plasmon mode **(Figure 2)**.

For example, the absorption spectra of nanoparticle with different aspect ratios have been simulated, and it is shown that the increase of aspect ratio would dramatically increase the wavelength. From the result by EL-Sayed et al., the maximum peak of longitude plasmon band displayed red shift from 650 to 800 nm after altering the ratio aspect from 2.6 to 3.6 [21]. For nanoparticles beyond these spheres and spheroids, particle shape plays a significant role in determining the LSPR spectrum.

The plasmonic spectrum would also rely on many other factors, such as the local medium surrounding. The LSPR wavelength shift is in accordance with the refractive index change and follows the relation as
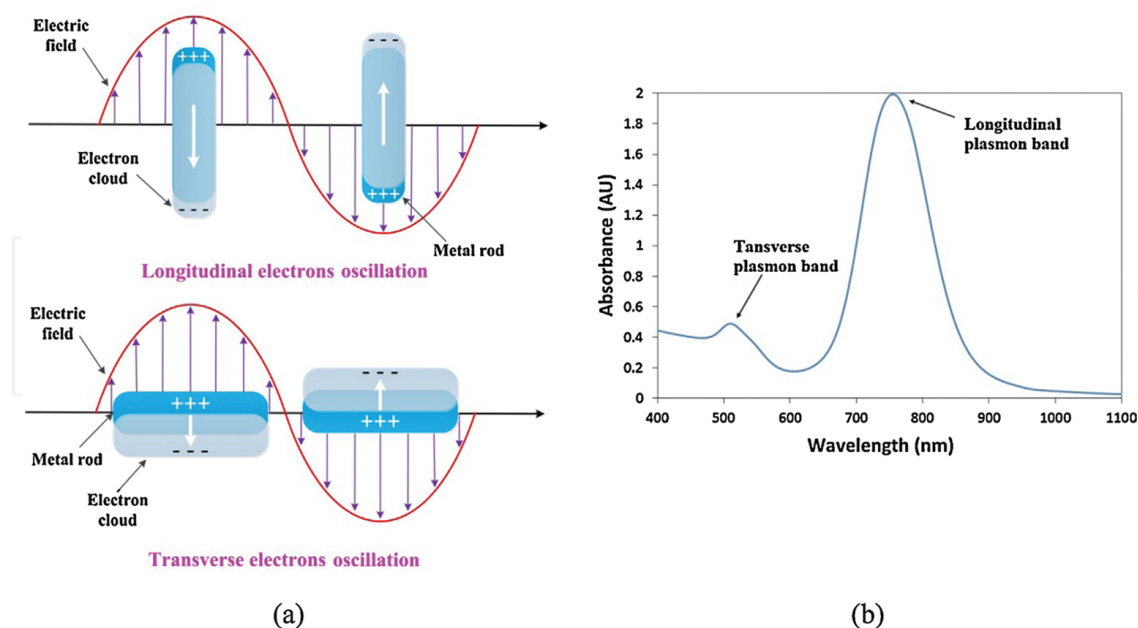
Figure 2. An illustration of LSPR excitation for prolate spheroid. The discrepant oscillation of electrons at longitudinal and transverse plasmon bands results in different plasmonic spectra [20].

$$\Delta\lambda = \text{m}\Delta n \left[1 - \exp\left(\frac{-2d}{l_d} \right) \right] \qquad (25)$$

where m represents the sensitivity factor (measured in nm per refractive index unit), Δn is the change of the refractive index, d indicates the effective thickness of the absorbed layer, and l_d denotes the characteristic electromagnetic field decay.

The complication of LSPR contributes to its potential applications only if we have gained a thorough understanding. Currently, there are several numerical methods for simulation of LSPR occurring at the surface of nanoparticles, including finite-difference time-domain (FDTD), discrete dipole approximation (DDA), and finite element method (FEM) [15]. An example of FDTD simulation will be illustrated in Section 5.

3. Fabrication of nanoparticles

The extensive studies on the fabrication of nanoparticles have promoted the potential application of LSPR. A reliable and reproducible synthesis method of nanostructures is the basis for LSPR detector. While the spherical nanoparticle of a noble metal is most readily prepared, it takes efforts to fabricate other desired structures. Several ways to fabricate desired nanostructure are illustrated in this section [22].

3.1. Citrate reduction

Citrate reduction is the most widely applied method for producing nanoparticles. The delicate addition of a calculated amount of citrate solution into the boiling metallic salt (such as HAuCl$_4$) solution generates solutions containing nanoparticles. The size of the nanoparticle would be controlled through the ratio between the citrate and the gold salt, the reaction temperature, and the reaction time [23]. The simplicity of these reductions makes it the most popular method to form nanoclusters.

3.2. Electrochemical method

The preparation of high yield of nanoparticles was initially proposed through applying an electrochemical method which can produce both nanocluster and nanorod structures [24, 25]. While preparing the cluster structure is easier, the nanorod structure was first synthesized through this method by Wang et al. in the late 1990s [26]. The synthesis of nanorod was carried out using a two-electrode-type electrochemical cell containing a gold metal plate as the sacrificial anode and a platinum plate as cathode and the electrolytic solution containing a rod-inducting cationic surfactant cetyltrimethylammonium bromide (CTAB) and a cationic co-surfactant tetradodecylammonium bromide (TCAB). During the electrolysis, the gold metal anode was oxidized into AuBr$_4$ and subsequently formed complexes with the cationic surfactants. The gold nanoparticle was generated through the reduction process after the complexes migrated to the cathode. In order to control the aspect ratio, a silver plate was placed in a position behind the platinum cathode. The aspect ratio was found to be dependent on the concentration and the release rate of the silver ions.

3.3. Electron beam lithography method

Electron beam lithography method is another common way used to generate metallic nano-structures. This method takes advantage of the precise control of the size, shape, and spatial distribution of the nanoparticles synthesized [27, 28]. Nevertheless, the lithography applied in this method makes it highly time-consuming owing to the small region processed.

3.4. Seed-mediated growth method

For the synthesis of nanostructure with specific aspect ratio, the seed-mediated growth method is the most used and has been extensively utilized [29, 30]. The method possesses merits such as the simplicity of the experiment, the high yield and high quality of produced nanorods, the convenience of size control, and the flexibility in structural modifications [31]. Lately, nano-structures such as 2D gold nanorings [32], composite core-shell nanorod [33], and branched gold nanodendrites [34] have been reported applying this experimental approach.

The seed-mediated growth method for nanorod structure was initially demonstrated by Jana et al. [35]. In their early experiment, the seed solution was prepared by the reduction of gold salt (HAuCl$_4$) with NaBH$_4$ in the presence of sodium citrate. The produced nanoparticles usually have a diameter of 3–4 nm and were used as the seeds by being added to the so-called growth solution, which was composed of HAuCl$_4$, cetyltrimethylammonium bromide (CTAB),

ascorbic acid, and AgNO$_3$. The latter three compositions acted as the template, the reducing agent, and the shape induction agent, respectively. The nanoparticle can subsequently grow into various aspect ratios by controlling the ratio of seed solution to the growth solutions.

The method was further improved later by the same group to obtain larger aspect ratio [36]. The seed and the growth solutions were prepared similarly except for adding AgNO$_3$. After adding the seed solution to the growth solution, the generated nanostructure was again used as seed with a repeated step. Despite nanostructures with larger aspect ratio acquired, by-products resulted from the reaction become significant, and more difficult purification processes are required in this process [37].

Based on the prototype, a wealth of significant improvements has been thereafter accomplished. For example, Nikoobakht et al. synthesized high-quality and high-yield nanorods by replacing the sodium citrate and adjusting the concentration of silver ions [38]. Ye et al. employed aromatic additives and a low CTAB concentration to achieve a broadly tunable localized plasmon band with higher purity [39].

Above all, mastering nanostructure is becoming more and more feasible, which has significantly advanced the applications of LSPR in molecular spectroscopy.

4. Nanoparticle LSPR sensor and detector

There are a wide variety of designs of LSPR detectors because the LSPR is more readily to be excited compared to the surface plasmon on a planar surface. The LSPR detector can be typically designed as either substrate-based or solution-based. We will hereby introduce three most widely studied structures: chip-based, optical-fiber-based, and solution-phase-based.

4.1. Chip-based LSPR sensor and detector

The chip-based LSPR detector can be fabricated by immobilizing nanostructures on the surface of a substrate, such as a glass slide and cover slip. The detector chip is easily achieved when nanostructures are produced through electron beam lithography technique or are grown on the substrate.

If the nanoparticles are produced in solution, such as citrate reduction, they can be immobilized on the surface through electrostatic force [40]. For instance, a clean glass substrate can be coated with polyelectrolyte that shows opposite charge to the surface charge of the generated nanoparticles. The charged substrate is subsequently immersed into the nanoparticle solution to attract nanoparticles by electrostatic force. However, the LSPR detector prepared in this way suffers from poor stability and poor uniformity.

Another method is based on the SAM technique [41]. A clean substrate is dipped into an alkylsilane solution, such as MPTMS, to form a thiol-terminated silane membrane on the surface. The silanized substrate surface would subsequently form covalent bonds with single layer of nanoparticles.

4.2. Optical fiber-based LSPR sensor and detector

Optical fiber-based LSPR detector is typically fabricated by immobilizing nanoparticles on the decladed fiber core of a multimode or single-mode optical fiber [42, 43]. Optical fiber-based LSPR detector shows advantages such as small sample volume, simple optical design, and minor electromagnetic interference [44].

4.3. Solution-phase-based LSPR sensor and detector

Solution-phase-based LSPR detectors are the nanoparticles suspended in solution rather than immobilized on a substrate, which makes the detection process of analytes inside the solution [45]. During the detection, the functional molecules should mix evenly with the nanoparticle solution and be closed enough to the surface of nanoparticles because of the decaying electric field.

5. LSPR-enhanced molecular spectroscopy

The utilization of localized surface plasmon resonance to enhance molecular spectroscopy has achieved prodigious enhancement factors. Applications of surface plasmon polariton include enhanced Raman spectrum [46], enhanced fluorescence [47], enhanced optical nano-devices [48], etc. Examples of the related experimental achievements are introduced and further elucidated through theoretical modeling applying Maxwell's equation.

5.1. Metal-enhanced fluorescence spectroscopy detecting polycyclic aromatic hydrocarbons

Oil spills are the major sea pollutants originating from tankers, offshore drilling rigs, etc. [49]. Spilled oil is toxic to living organisms, and even one spill oil would cause large mortality in the marine ecosystem [50]. The monitor of the water quality is crucial and demands trace amount detection technique. Polycyclic aromatic hydrocarbons are a major component of crude oil and would be selected as the surveillance target.

The easy-to-handle fluorescence spectroscopy is enhanced by LSPR during the detections of crude oil [51]. The silver nanoparticle solution was prepared with the citrate reduction method shown previously. The glass-based detector was prepared by (3-aminopropyl)trimethoxysilane-coated quartz substrates. Through the SEM image, an average grain size of 80 nm was analyzed over 200 particles, as shown in **Figure 3(a)**. The characteristic absorption spectrum of the silver nanoparticles has its peak at 405 nm as displayed in **Figure 3(b)**, resulting in LSPR at the surface of the silver nanoparticles.

The fluorescence spectrum of artificial diesel oil polluted seawater emulsions was measured in the presence and in the absence of the glass-based nanoparticles, as shown in **Figure 3(c)**. It is distinct that the maximum peak is enhanced with the intensity rising from 6×10^4 to more than 30×10^4, indicating an enhancement factor of 5.44.
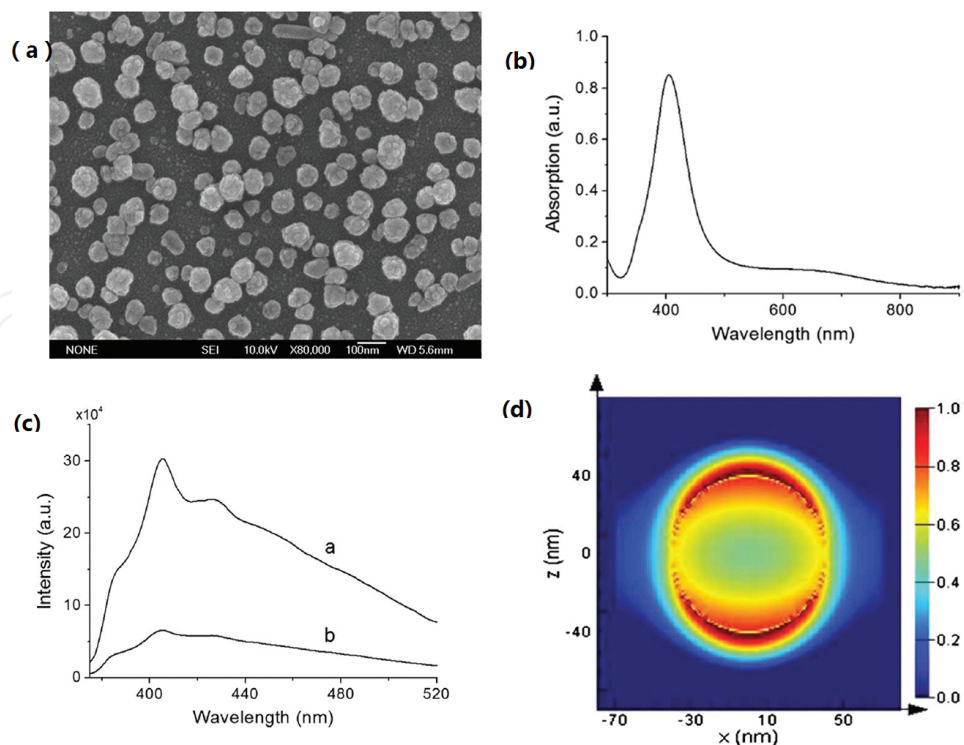
Figure 3. (a) SEM image shows the structure of the applied silver nanoparticles, (b) the absorption spectrum of silver nanoparticles at room temperature, (c) fluorescence spectra of diesel oil emulsions in artificial seawater before and after enhancement (emitted at 355 nm), and (d) the electric field enhancements of silver nanoparticles at 355 nm.

To understand the enhancement, the electric field effect could be modeled through FDTD method, as shown in **Figure 3(d)** with the near-field plotted. During the simulation, the excitation field is incident in the positive x-direction and polarized along the z-axis. The dipole resonance mode is the key to the enhancement in this case, which explains the enhanced fluorescence is resulted from the increased electric fields.

5.2. Enhanced Raman scattering

The enhancement effects of LSPR on Raman spectroscopy are generally attributed to the presence of hot spots on the rough particle surface, but there are more factors involved during this process, such as the complicated intraparticle coupling [52, 53]. Combined experiments and simulations are performed to interpret this issue.

The silver nanoparticles on quartz substrates were first synthesized through citrate reduction and applied to enhance the Raman spectrum of methylene blue. From the obtained spectra shown in **Figure 4**, it is obvious that the involvement of LSPR improves the resolution, where characteristic vibrational peaks are distinctly displayed. The enhancement factors are 3.2×10^5 and 1.3×10^7 for SERS excited by a 514.5 nm Ar-ion laser and a 785 nm diode laser, respectively. Since the nanoparticles were attracted by (3-aminopropyl)trimethoxysilane with SAM method, it is estimated that they lay as one layer instead of taking the form of aggregation. However, it is notable that the enhancement factor was higher than theoretically estimated for spherical particles [54]. More sophisticated explanation should be accounted.
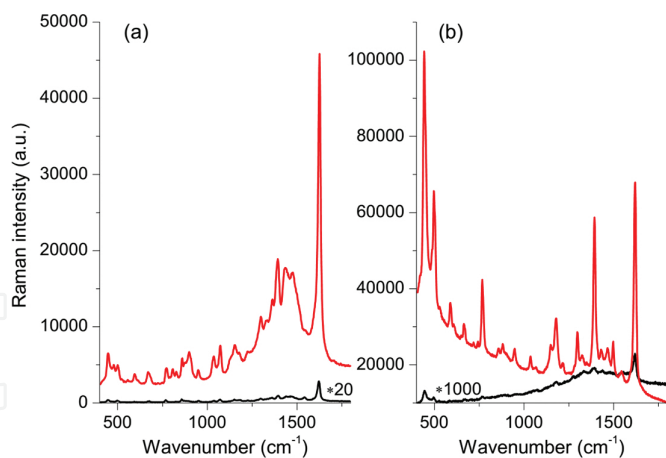
Figure 4. (a) The Raman spectra of methylene blue excited by 514.5 nm in the absence (black) and the presence (red) of SERS substrates and (b) the Raman spectra of methylene blue excited by 785 nm in the absence (black) and the presence (red) of SERS substrates.

SEM image shown in **Figure 5(a)** indicates that the submicrometer silver particles are flowerlike with distinct surface protrusions. The average diameter of the silver particles is analyzed to be about 500 nm. Three-dimensional finite-difference time-domain (FDTD) method was employed to calculate both far- and near-field optical properties of the submicrometer silver particles. The control structure, i.e., the smooth spherical structure, and the mimicking structure, i.e., a large particle (D = 400 nm) with 26 small spherical particles (D = 100 nm) evenly distributed on the exterior surface, were modeled.
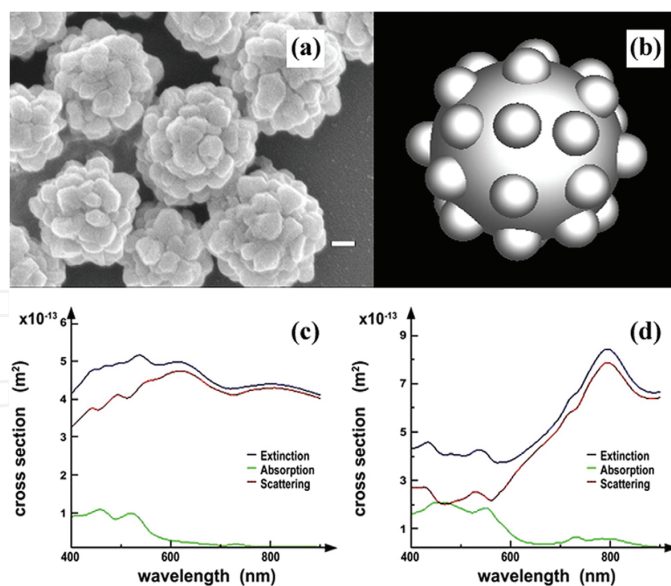

Figure 5. (a) The SEM image of rough submicrometer silver particles. Scale bar: 100 nm. (b) Schematic diagram of the rough submicrometer silver particle model. The 26 small peripheral particles were submerged into the large core particle, effectively generating many hemispheres on the surface. (c) Calculated extinction, absorption, and scattering spectra of the smooth silver particles model. (d) Calculated extinction, absorption, and scattering spectra of the rough silver particle model.

The characteristic spectra of both models are illustrated in **Figure 5(c)** and **(d)**. It is noteworthy that the extinction spectrum of the smooth particle shows featured bands originated from dipole resonance (ca. 800 nm) and higher-order multipole resonances, such as quadrupole resonance (ca. 620 nm), while the featured band of rough particles located at ca. 800 nm. The dipole field at the surface of rough particles is intensified through scattering. The augmented enhancement factor at 785 nm in the SERS spectrum is thus interpreted.

Understanding the wavelength dependence of SERS requires the distribution of electric fields of metal particles, as shown in **Figure 6**. The different electric distributions at different wavelengths for the smooth surface point out that the enhancement effect under the shorter wavelength (514.5 nm) originates from the multipole effect, while the longer wavelength (785 nm) is resulted from the dipole effect. The electric distribution for the rough surface denotes the prominent near-field enhancement at the rough surface because of a more localized distribution of the particle's conduction electrons.
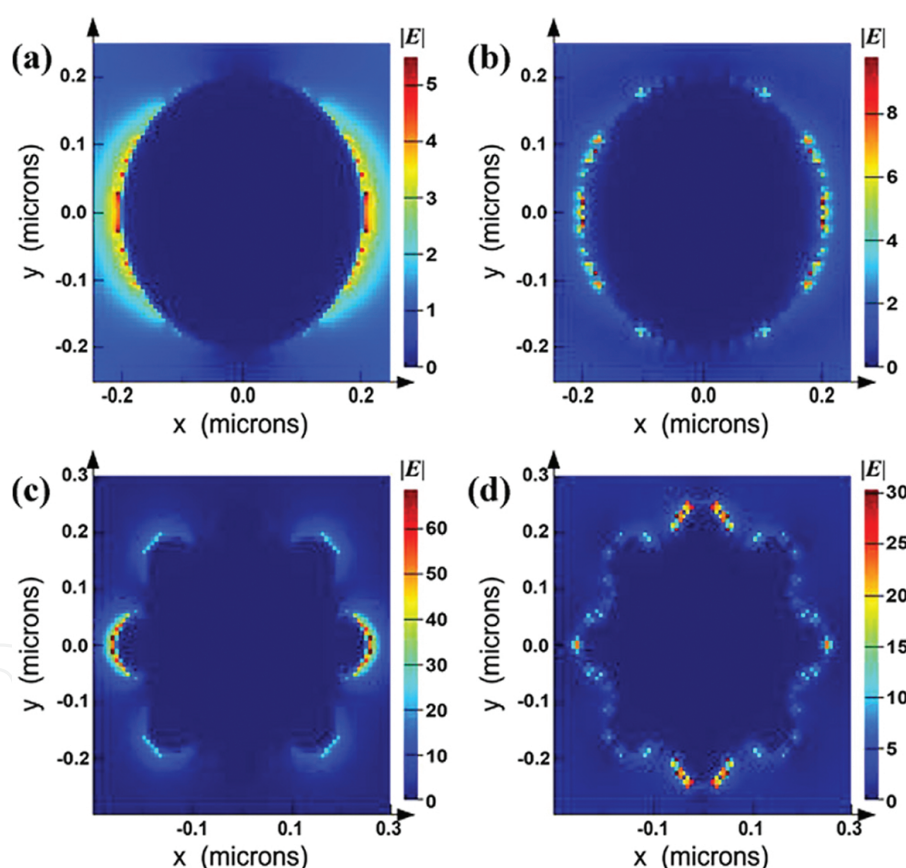

Figure 6. The distribution of electric fields around the silver particle model through FDTD calculation. The excitation field is incident in the positive z-direction. (a) and (b) The smooth silver particle model excited by 785 and 514.5 nm, respectively. (c) and (d) The rough silver particle model excited by 785 and 514.5 nm, respectively.

Further verification of the theoretical computed electric field is accomplished through near-field scanning optical microscopy (NSOM), which can measure the intensity distribution of optical fields of the rough submicrometer silver particles on a quartz slide, as shown in

Figure 7. The rough submicrometer silver particle shows a strong optical field distribution, shedding light on the stronger enhancement factor.
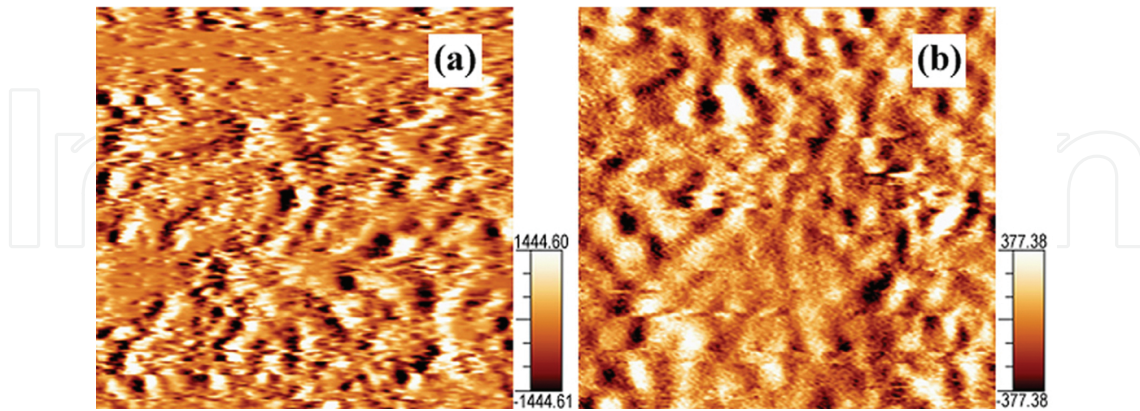

Figure 7. The measured intensity distribution of optical fields on the surface of nanoparticles by NSOM under 785 nm excitation. (a) Rough submicrometer silver particles and (b) spherical silver nanoparticles.

In order to illustrate the enhancement of electric field with a formula, the total electric field ($\vec{E}_{Total}$) of LSPR is accounted as the sum of radiation field produced by LSPR of the core particle ($\vec{E}_o$) and the peripheral particles ($\vec{E}_i$), as

$$\vec{E} = \vec{E}_o + \sum_{i=1}^{n} \chi_i(\mathbf{r}_i) \vec{E}_i \tag{26}$$

where $\chi_i(\mathbf{r}_i)$ is the weighing factor for the *ith* peripheral particles at $\mathbf{r}_i$.

Based on the equation of the radiation field produced by the dipole resonance, the constant phase difference could be found for the radiation waves of large core particle and small peripheral for a direction r ($R\cos\theta_i$). Electric field from the core particle ($\vec{E}_o$) and the peripheral particles ($\vec{E}_i$) can be demonstrated and $\vec{E}_{Total}$ can be rewritten as

$$\vec{E}_o = \frac{k^2 P_o \sin(\alpha)}{4\pi\varepsilon_0 r} e^{ikr} \tag{27}$$

$$\vec{E}_i = \frac{k^2 P \sin(\alpha)}{4\pi\varepsilon_0 r} e^{ik(r + R\cos\theta_i)} \tag{28}$$

$$\vec{E}_{Total}^2 = E_o{}^2 + \chi_i{}^2 E_i{}^2 + 2\chi_i E_o E_i \cos(kR\cos\theta_i) \tag{29}$$

where ε_0 represents the permittivity of vacuum, P_o denotes the dipole moment of the large core particle, k expresses the wave number of the radiation field, and α is the angle between the incident and radiation fields. The effect of the roughness of the surface would be described by different induced dipole moments, as

$$P = E_{ex}a^3\frac{\varepsilon_{np} - \varepsilon_0}{\varepsilon_{np} + 2\varepsilon_0} \tag{30}$$

In here, a is the radius of the particle, E_{ex} represents the incident electric field, and ε_{np} and ε_o denote the relative permittivity of the particle and the surrounding medium, respectively. The dependence of dipole enhancement with the grain is thus illustrated. A more distinct demonstration can be achieved by simulation through controlling the different sizes of peripheral particles, as shown in **Figure 8**, which indicates the enhanced induced dipole moment with larger peripheral particles.
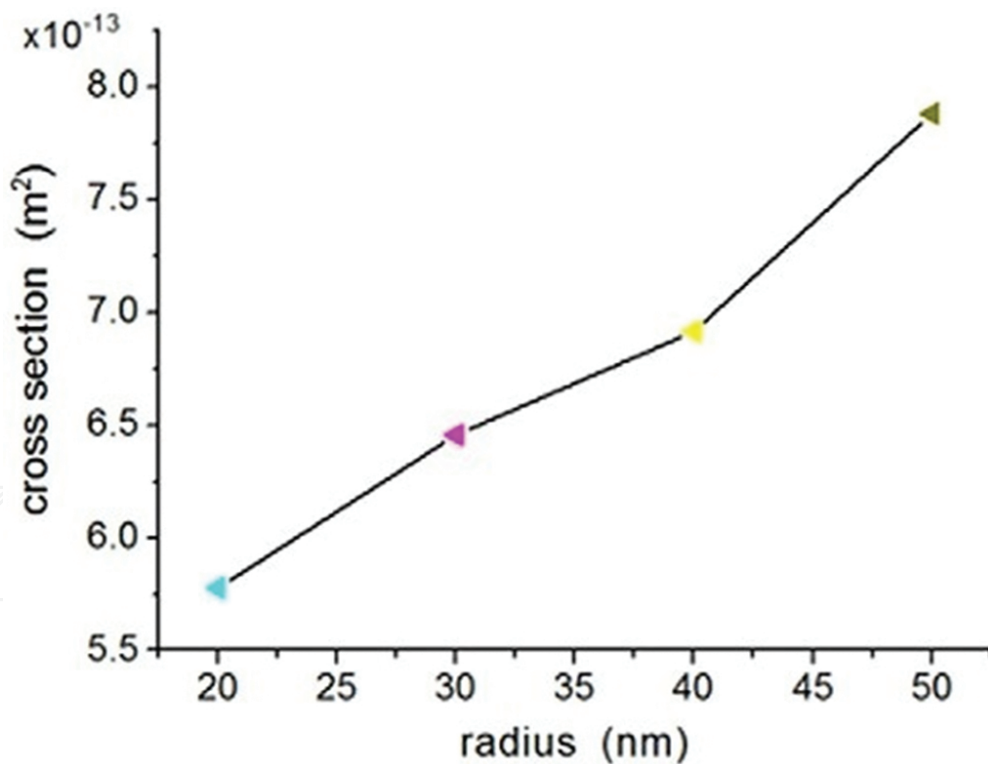

Figure 8. Enhanced dipole mode of LSPR with the increasing radius of the peripheral particles.

The effects of a rough surface are thus thoroughly studied combining experiment and theoretical calculation. The enlightening result indicating how small particles affect the enhancement factor helps further design more advanced nanoparticle detectors.

6. Conclusion

The localized surface plasmon resonance taking advantage of easy excitation is becoming increasing popular in the application of molecular spectroscopy, which has improved the resolution of spectroscopy and makes detection limit as low as femtogram. As we show in this chapter, there are numerous techniques to synthesize the desired nanostructures nowadays, and LSPR derived from those nanoparticles has demonstrated considerable enhancement factor to improve the applicability of molecular spectroscopy involving fluorescence, the Raman scattering, etc. On the one hand, it is to design better nanoparticles that arise localized surface plasmon; on the other hand, the mechanism of resulting electric field on the surface of nanoparticle needs to be accounted for different nanostructures. The multifactor-determined LSPR can now be currently elaborated through FDTD method. The joint experimental data with theoretical perspective are beneficial for a better understanding of the characteristic of LSPR and the resulting enhancement factor. Further intensive studies on LSPR combining experiments and modeling will broaden the application of LSPR and favor spectroscopies at molecular precision.

Acknowledgements

Author details

Lu Sun, Ping Chen[*] and Lie Lin

*Address all correspondence to: chping@nankai.edu.cn

Key Laboratory of Optoelectronic Information Science and Technology, Ministry of Education of China, Institute of Modern Optics, Nankai University, Tianjin, China

References

[1] Wozniak, A.K., Schroder, G.F., Grubmuller, H., Seidel, C.A., Oesterhelt, F. Single-molecule FRET measures bends and kinks in DNA. Proc Natl Acad Sci U S A. 2008;105(47):18337-18342. DOI: 10.1073/pnas.0800977105

[2]   Fujisawa, T., Kuramochi, H., Hosoi, H., Takeuchi, S., Tahara, T. Role of coherent low frequency motion in excited-state proton transfer of green fluorescent protein studied by timeresolved impulsive stimulated raman spectroscopy. J Am Chem Soc. 2016;138(12):3942–3945. DOI: 10.1021/jacs.5b11038 19

[3]   Shi, X., Beauchamp, K.A., Harbury, P.B., Herschlag, D From a structural average to the conformational ensemble of a DNA bulge. Proc Natl Acad Sci U S A. 2014;111(15): 1473-1480. DOI: 10.1073/pnas.1317032111

[4]   Salmon, L., Nodet, G., Ozenne, V., Yin, G., Jensen, M.R., Zweckstetter, M., Blackledge, M. NMR characterization of long-range order in intrinsically disordered proteins. J Am Chem Soc. 2010;132(24):8407-8408. DOI: 10.1021/ja101645g

[5]   Agirrezabala, X., Liao, H.Y., Schreiner, E., Fu, J., Ortiz-Meoz, R.F., Schulten, K., Green, R., Frank, J. Structural characterization of mRNA-tRNA translocation intermediates. Proc Natl Acad Sci U S A. 2012;109(16):6094-6099. DOI: 10.1073/pnas.1201288109

[6]   Kneipp, K., Kneipp, H., Kneipp, J. Surface-enhanced Raman scattering in local optical fields of silver and gold nanoaggregates—from single-molecule Raman spectroscopy to ultrasensitiveprobing in live cells. Acc Chem Res. 2006;39(7):443-450. DOI: 10.1021/ar050107x

[7]   El-Sayed, M.A. Some interesting properties of metals confined in time and nanometer space of different shapes. Acc Chem Res. 2001;34(4):257-264. DOI: 10.1021/ar960016n

[8]   Rosi, N.L., Mirkin, C.A. Nanostructures in biodiagnostics. Chem Rev. 2005;105(4): 1547-1562. DOI: 10.1021/cr030067f

[9]   Chen, H.J., Kou, X.S., Yang, Z., Ni, W.H., Wang, J.F. Shape- and size-dependent refractive index sensitivity of gold nanoparticles. Langmuir. 2008;24(10):5233-5237. DOI: 10.1021/la800305j

[10] Hu, M., Chen, J.Y., Li, Z.Y., Au, L., Hartland, G.V., Li, X.D., Marquez, M., Xia, Y.N. Gold nanostructures: engineering their plasmonic properties for biomedical applications. Chem Soc Rev. 2006;35(11):1084-1094. DOI: 10.1039/B517615h

[11] Zhang, P., Haslett, T.L., Douketis, C., Moskovits, M. Mode localization in self-affine fractal interfaces observed by near-field microscopy. Phys Rev B. 1998;57(24): 15513-15518. DOI: 10.1103/PhysRevB.57.15513

[12] Reinhard, B.M., Sheikholeslami, S., Mastroianni, A., Alivisatos, A.P., Liphardt, J. Use of plasmon coupling to reveal the dynamics of DNA bending and cleavage by single EcoRV restriction enzymes. Proc Natl Acad Sci U S A. 2007;104(8):2667-2672. DOI: 10.1073/pnas.0607826104

[13] Sonnichsen, C., Reinhard, B.M., Liphardt, J., Alivisatos, A.P. A molecular ruler based on plasmon coupling of single gold and silver nanoparticles. Nat Biotechnol. 2005;23(6): 741-745. DOI: 10.1038/nbt1100

[14] Yu, W.W. and White, I.M. Inkjet-printed paper-based SERS dipsticks and swabs for trace chemical detection. Analyst. 2013;138(4):1020-1025. DOI: 10.1039/c2an36116g

[15] Zhao, J., Pinchuk, A.O., Mcmahon, J.M., Li, S.Z., Ausman, L.K., Atkinson, A.L., Schatz, G.C. Methods for describing the electromagnetic properties of silver and gold nano-particles. Acc Chem Res. 2008;41(12):1710-1720. DOI: 10.1021/ar800028j

[16] Wood, R.W. On a remarkable case of uneven distribution of light in a diffraction grating spectrum. Proc Phys Soc Lond 1902;18:269. DOI: 10.1088/1478-7814/18/1/325

[17] Willets, K.A. and Van Duyne, R.P.. Localized surface plasmon resonance spectroscopy and sensing. Annu Rev Phys Chem 2007;58:267-297. DOI: 10.1146/annurev.physchem. 58.032806.104607

[18] Anderson, L.J.E., Mayer, K.M., Fraleigh, R.D., Yang, Y., Lee, S., Hafner, J.H. Quantitative measurements of individual gold nanoparticle scattering cross sections. J Phys Chem C. 2010;114(25):11127-11132. DOI: 10.1021/jp1040663

[19] Jensen, T.R., Duval, M.L., Kelly, K.L., Lazarides, A.A., Schatz, G.C., Van Duyne, R.P. Nanosphere lithography: effect of the external dielectric medium on the surface plasmon resonance spectrum of a periodic array of sliver nanoparticles. J Phys Chem B. 1999;103(45):9846-9853. DOI: 10.1021/Jp9926802

[20] Cao, J., Sun, T., Grattan, K.T.V. Gold nanorod-based localized surface plasmon reso-nance biosensors: a review. Sens Actuat B Chem. 2014;195:332-351. DOI: 10.1016/j.snb. 2014.01.056

[21] Link, S., Mohamed, M.B., El-Sayed, M.A.. Simulation of the optical absorption spectra of gold nanorods as a function of their aspect ratio and the effect of the medium dielectric constant. J Phys Chem B. 1999;103(16):3073-3077. DOI: 10.1021/Jp990183f

[22] Petryayeva, E., Krull, U.J. Localized surface plasmon resonance: nanostructures, bioassays and biosensing—a review. Anal Chim Acta. 2011;706(1):8-24. DOI: 10.1016/ j.aca.2011.08.020

[23] Daniel, M.C., Astruc, D. Gold nanoparticles: assembly, supramolecular chemistry, quantum size-related properties, and applications toward biology, catalysis, and nanotechnology. Chem Rev. 2004;104(1):293-346. DOI: 10.1021/cr030698+

[24] Hammons, J.A., Ustarroz, J., Muselle, T., Torriero, A.A.J., Terryn, H., Suthar, K., Ilavsky, J. Supported silver nanoparticle and near-interface solution dynamics in a deep eutectic solvent. J Phys Chem C. 2016;120(3):1534-1545. DOI: 10.1021/acs.jpcc.5b09836

[25] Lu, W.S., Wang, H.F., Zhang, J.P., Jiang, L. Gold nanorods: synthesis, growth mechanism and purification. Prog Chem. 2015;27(7):785-793. DOI: 10.7536/PC150111

[26] Chang, S.S., Shih, C.W., Chen, C.D., Lai, W.C., Wang, C.R.C. The shape transition of gold nanorods. Langmuir. 1999;15(3):701-709. DOI: 10.1021/La980929l

[27] Boltasseva, A. Plasmonic components fabrication via nanoimprint. J Opt A Pure Appl Opt. 2009;11(11):114001. DOI: 10.1088/1464-4258/11/11/114001

[28] Zhang, X.Y., Whitney, A.V., Zhao, J., Hicks, E.M., Van Duyne, R.P. Advances in contemporary nanosphere lithographic techniques. J Nanosci Nanotechnol. 2006;6(7): 1920-1934. DOI: 10.1166/jnn.2006.322

[29] Feng, L.L., Xuan, Z.W., Ma, J.B., Chen, J., Cui, D.X., Su, C.W., Guo, J.M., Zhang, Y.J. Preparation of gold nanorods with different aspect ratio and the optical response to solution refractive index. J Exp Nanosci. 2015;10(4):258-267. DOI: 10.1080/17458080.2013.824619

[30] Satija, J., Tharion, J., Mukherji, S. Facile synthesis of size and wavelength tunable hollow gold nanostructures for the development of a LSPR based label-free fiber-optic biosensor. RSC Adv. 2015;5(86):69970-69979. DOI: 10.1039/c5ra13941d

[31] Zhang, D.J., Zhang, C.Y., Lu, Y., Hao, Y.W., Liu, Y.Q. Preparation of Au@ Ag core-shell nanoparticles through seed-mediated growth method. Prog Chem. 2015;27(8): 1057-1064. DOI: 10.7536/PC150140

[32] Jang, H.J., Ham, S., Acapulco, J.A.I., Song, Y., Hong, S., Shuford, K.L., Park, S. Fabrication of 2D Au nanorings with Pt framework. J Am Chem Soc. 2014;136(50):17674-17680. DOI: 10.1021/ja510916y

[33] Ma, Y.N., Zhou, J., Shu, L., Li, T.H., Petti, L., Mormile, P. Optimizing Au/Ag core-shell nanorods:purification, stability, and surface modification. J Nanopart Res. 2014;16(6): 2439. DOI: 10.1007/S11051-014-2439-6

[34] Jia, W.F., Li, J.R., Jiang, L. Synthesis of highly branched gold nanodendrites with a narrow size distribution and tunable NIR and SERS using a multiamine surfactant. ACS Appl Mater Inter. 2013;5(15):6886-6892. DOI: 10.1021/am401006b

[35] Jana, N.R., Gearheart, L., Murphy, C.J. Seed-mediated growth approach for shape-controlled synthesis of spheroidal and rod-like gold nanoparticles using a surfactant template. Adv Mater. 2001;13(18):1389-1393. DOI: 10.1002/1521-4095

[36] Jana, N.R., Gearheart, L., Murphy, C.J. Wet chemical synthesis of high aspect ratio cylindrical gold nanorods. J Phys Chem B. 2001;105(19):4065-4067. DOI: 10.1021/ Jp0107964

[37] Huang, X.H., Neretina, S., El-Sayed, M.A. Gold nanorods: from synthesis and properties to biological and biomedical applications. Adv Mater. 2009;21(48):4880-4910. DOI: 10.1002/adma.200802789

[38] Nikoobakht, B., El-Sayed, M.A. Preparation and growth mechanism of gold nanorods (NRs) using seed-mediated growth method. Chem Mater. 2003;15(10):1957-1962. DOI: 10.1021/cm0207321

[39] Ye, X.C., Jin, L.H., Caglayan, H., Chen, J., Xing, G.Z., Zheng, C., Doan-Nguyen, V., Kang, Y.J., Engheta, N., Kagan, C.R., Murray, C.B. Improved size-tunable synthesis of

monodisperse gold nanorods through the use of aromatic additives. ACS Nano. 2012;6(3):2804-2817. DOI: 10.1021/nn300315j

[40] Gole, A., Murphy, C.J. Polyelectrolyte-coated gold nanorods: synthesis, characterization and immobilization. Chem Mater. 2005;17(6):1325-1330. DOI: 10.1021/cm048297d

[41] Marinakos, S.M., Chen, S.H., Chilkoti, A. Plasmonic detection of a model analyte in serum by a gold nanorod sensor. Anal Chem. 2007;79(14):5278-5283. DOI: 10.1021/ac0706527

[42] Cheng, S.F., Chau, L.K. Colloidal gold-modified optical fiber for chemical and biochemical sensing. Anal Chem. 2003;75(1):16-21. DOI: 10.1021/ac020310v

[43] Tang, J.L., Cheng, S.F., Hsu, W.T., Chiang, T.Y., Chau, L.K. Fiber-optic biochemical sensing with a colloidal gold-modified long period fiber grating. Sens Actuat B Chem. 2006;119(1):105-109. DOI: 10.1016/j.snb.2005.12.003

[44] Cao, J., Galbraith, E.K., Sun, T., Grattan, K.T.V. Cross-comparison of surface plasmon resonance-based optical fiber sensors with different coating structures. IEEE Sens J. 2012;12(7):2355-2361. DOI: 10.1109/Jsen.2012.2188713

[45] Yu, C.X., Irudayaraj, J. Multiplex biosensor using gold nanorods. Anal Chem. 2007;79(2):572-579. DOI: 10.1021/ac061730d

[46] Gawinkowski, S., Pszona, M., Gorski, A., Niedziolka-Jonsson, J., Kaminska, I., Nogala, W., Waluk, J. Single molecule Raman spectra of porphycene isotopologues. Nanoscale. 2016;8(6):3337-3349. DOI: 10.1039/c5nr08627b

[47] Shen, Y.B., He, T., Wang, W.H., Zhan, Y.L., Hu, X., Yuan, B.F., Zhou, X.C. Fluorescence enhancement on silver nanoplates at the single- and sub-nanoparticle level. Nanoscale. 2015;7(47):20132-20141. DOI: 10.1039/c5nr06146f

[48] Shen, W.F., Tang, J.G., Wang, D., Yang, R.Q., Chen, W.C., Bao, X.C., Wang, Y., Jiao, J.Q., Wang, Y.X., Huang, Z., Huang, L.J., Liu, J.X., Wang, W., Wu, P.H., Belfiore, L.A. Enhanced efficiency of polymer solar cells by structure-differentiated silver nanodopants in solution-processed tungsten oxide layer. Mater Sci Eng B Adv. 2016;206:61-68. DOI: 10.1016/j.mseb.2015.11.004

[49] Rogowska, J., Namiesnik, J. Environmental implications of oil spills from shipping accidents. Rev Environ Contam Toxicol. 2010;206:95-114. DOI: 10.1007/978-1-4419-6260-7_5

[50] Mearns, A.J., Reish, D.J., Oshida, P.S., Ginn, T., Rempel-Hester, M.A., Arthur, C., Rutherford, N., Pryor, R. Effects of pollution on marine organisms. Water Environ Res. 2015;87(10):1718-1816. DOI: 10.2175/106143015X14338845156380

[51] Zhang, F., Zhang, L., Mao, S.C., Chen, P., Cui, J.C., Tang, Y.G., Wang, K., Lin, L., Qi, X.D. Use of metal-enhanced fluorescence spectroscopy for detection of polycyclic aromatic

hydrocarbons in diesel oil emulsions in artificial seawater. Environ Technol. 2012;33(18):2071-2075. DOI: 10.1080/09593330.2012.660643

[52] Zhang, F., Chen, P., Zhang, L., Mao, S.C., Lin, L., Tang, Y.G., Cui, J.C., Qi, X.D., Yang, J.H., Ma, Y.F. Enhancement of Raman scattering by field superposition of rough submicrometer silver particles. Appl Phys Lett. 2012;100(17):4705083. DOI: 10.1063/1.4705083

[53] Bok, H.M., Shuford, K.L., Jeong, E., Park, S. Intra-surface plasmon coupling between smooth and nanoporous blocks in a gold nanorod. Chem Commun. 2010;46(6):982-984. DOI: 10.1039/b918510k

[54] Kerker, M. Estimation of surface-enhanced Raman scattering from surface-averaged electromagnetic intensities. J. Colloid Interface Sci.. 1987;18:417-421. DOI: 10.1016/0021-9797(87)90477-2